Available online at www.sciencedirect.com

ScienceDirect

Geochimica et Cosmochimica Acta 170 (2015) 188–203

Geochimica et Cosmochimica Acta

www.elsevier.com/locate/gca

Using $^{224}Ra/^{228}Th$ disequilibrium to quantify benthic fluxes of dissolved inorganic carbon and nutrients into the Pearl River Estuary

Pinghe Cai *, Xiangming Shi, Qingquan Hong, Qing Li, Lingfeng Liu, Xianghui Guo, Minhan Dai

State Key Laboratory of Marine Environmental Science, Xiamen University, Xiamen 361005, PR China
College of Ocean and Earth Sciences, Xiamen University, Xiamen 361005, PR China

Received 10 February 2015; accepted in revised form 26 August 2015; Available online 5 September 2015

Abstract

The $^{224}Ra/^{228}Th$ disequilibrium that was recently observed in coastal sediments has been proven to be an excellent proxy for tracing the benthic processes that regulate solute transfer across the sediment–water interface. In order to better utilize this proxy, there is a need to understand the reaction kinetics of ^{224}Ra in sediments. In this study, depth profiles of ^{224}Ra and ^{228}Th in bulk sediments were collected along a transect in the Pearl River Estuary (PRE). Together with bulk sediment measurements, dissolved ^{224}Ra, dissolved inorganic carbon (DIC), and nutrients ($NO_2^- + NO_3^-$, NH_4^+) in pore water and in the overlying waters were also determined. A marked deficit of ^{224}Ra with respect to ^{228}Th with large spatial variations was observed in the PRE sediments. By use of a diagenetic model for the distributions of dissolved and adsorbed ^{224}Ra in sediments, we infer that adsorption removes ^{224}Ra from aqueous phase at a rate of 0.1 ± 1.1–2000 ± 400 d^{-1}. In addition, adsorption of ^{224}Ra exhibits a rate sequence of oxic freshwater > anoxic freshwater > anoxic brackish water, probably reflecting the effect of the redox conditions and ionic strength on the adsorption–desorption kinetics of ^{224}Ra.

Benthic fluxes of ^{224}Ra were estimated from the observed deficit of ^{224}Ra in the sediments using a one-dimensional (1D) mass balance exchange model. We demonstrated that irrigation was the predominant process that controls solute transfer across the sediment–water interface, whereas molecular diffusion and sediment mixing together contributed <5% of the total ^{224}Ra fluxes from bottom sediments. We then utilized the $^{224}Ra/^{228}Th$ disequilibrium approach to quantify the benthic fluxes of DIC and nutrients. We showed that sediment interstitial waters delivered approximately $42 \pm 6 \times 10^9$ mol of DIC and ~16 $\pm 1 \times 10^9$ mol of NH_4^+ into the PRE in the dry season. In contrast, it removed about $13 \pm 1 \times 10^9$ mol of NO_3^- from the overlying water column. The benthic flux of DIC is equivalent to ~18% of the riverine input in this season. In terms of nutrients, our results suggest that bottom sediments are a major sink of water column NO_3^-, and are a predominant source of NH_4^+ in the PRE. Overall, this study indicates that irrigation is an important process and must be considered in the mass balance of DIC and nutrients in estuaries.

1. INTRODUCTION

Exchange of sediment interstitial waters with the water column has long been considered a major source of many chemical species in estuaries (e.g., Knox et al., 1981).

* Corresponding author at: State Key Laboratory of Marine Environmental Science, Xiamen University, Xiamen 361005, PR China. Tel.:+86 592 2880179; fax: +86 592 2180655.
E-mail address: Caiph@xmu.edu.cn (P. Cai).

http://dx.doi.org/10.1016/j.gca.2015.08.015
0016-7037/

However, release rates of these species from estuarine sediments remain poorly constrained, due primarily to limitations inherent in the traditional approaches for quantifying the benthic fluxes across the sediment–water interface in dynamic coastal settings, i.e., the benthic chamber method and the modeling approach (e.g., Hensen et al., 2006). The newly developed $^{224}Ra/^{228}Th$ disequilibrium approach utilizes the deficit of ^{224}Ra with respect to ^{228}Th in near-surface sediments to determine the ^{224}Ra flux across the sediment–water interface. By combining the concentration gradient of ^{224}Ra in pore water with the concentration gradient of the dissolved species of interest at the interface, the ^{224}Ra flux is converted into a benthic flux of that species (Cai et al., 2012, 2014). This approach does not impose any interference on the system and is particularly suitable for studies on the benthic exchange in estuaries, where a marked deficit of ^{224}Ra with respect to ^{228}Th is observed in the near-surface sediments (Cai et al., 2014).

In this study, we take advantage of $^{224}Ra/^{228}Th$ disequilibrium to quantify benthic fluxes of dissolved inorganic carbon (DIC) and nutrients ($NO_3^- + NO_2^-$, NH_4^+) in the Pearl River Estuary (PRE), southern China. DIC and nutrients are intimately involved in the biogeochemical processes in estuaries. As a consequence of diagenetic reactions, DIC and NH_4^+ concentrations are generally significantly elevated in sediment interstitial waters as compared to the overlying water column. In contrast, nitrate is generally depleted in anoxic interstitial waters due to a process termed denitrification. These biogeochemical reactions produce distinct chemical compositions in interstitial waters, making bottom sediments a potential source (or sink) of DIC and nutrients in estuarine waters. As such, there is a need to understand solute transport processes occurring at the sediment–water interface and to assess quantitatively, the role of interstitial water exchange in the water column budget of these constituents. As to the PRE, previous investigations have revealed that water column DIC and NH_4^+ concentrations in the upper estuary can be up to ~3000 and ~800 μM, respectively (Dai et al., 2006, 2008; Guo et al., 2008). However, the source of such high levels of DIC and NH_4^+ remains to be identified, and the role of bottom sediments in the water column budget of these constituents is yet to be evaluated.

2. SAMPLING AND ANALYSIS

2.1. Study area

The Pearl River is the 13th largest river in the world with a water discharge of $\sim 330 \times 10^9$ m^3 y^{-1} (Dai et al., 2014). It delivers $\sim 80 \times 10^6$ tons of sediments annually, most of which is believed to be trapped within the estuary (Liu et al., 2009). The river discharges to the South China Sea via three estuaries, Huangmaohai, Modaomen, and Lingdingyang, the last of which are traditionally referred to as the Pearl River Estuary (PRE). The PRE is a north–south bell-shaped estuary, with an axial length of ~70 km (Fig. 1). It has a narrow head of only several kilometers in the upper estuary and a relatively wide seaside entrance of ~50 km in the lower estuary. Water depth increases from

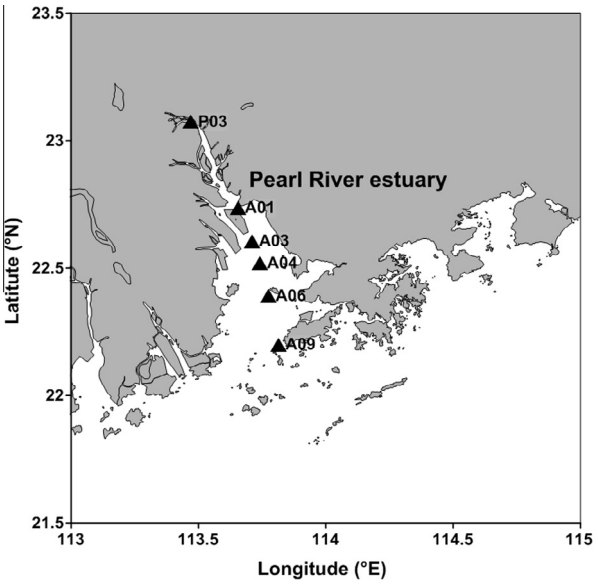

Fig. 1. Map of the Pearl River Estuary. Sampling stations are indicated by solid triangles.

~2.8 m in the upper estuary to ~20 m in the lower estuary. Tides are mainly semi-diurnal (M2) and diurnal (K1) around the PRE region. Tide amplitudes are typically 1–1.5 m within the estuary. Tides form a counter-clockwise tidal residual circulation and may affect the estuarine circulation on both tidal and sub-tidal frequencies (Mao et al., 2004). With the seaward freshwater discharge from the river, they lead to a gravitational circulation within the estuary. Consequently, the PRE is classified as a salt wedge estuary in the wet season (Lu and Gan, 2015).

The seabed of the PRE is dominated by fine-grained sediments. In the river mouth area, the bottom sediments are relatively coarse, but the mid- and lower estuary region contains a mixture of silt and clay (He et al., 2010; Zhang et al., 2013). Mollusca and polychaetes are the main benthic fauna in the PRE. Mollusca were identified to be the dominant species in spring and autumn. Based on the surveys conducted during 1980–2000, the average biomass of the benthic fauna varied between 7.4 and 30.1 g/m^2. Spatial variations in the biomass of the benthic fauna, however, were found to be large in this region. High biomass was generally observed in the mid-estuary region, which can be >80 g/m^2 (Huang et al., 2002).

2.2. Sample collection

Sediment and seawater samples were collected during a cruise to the PRE from 16 to 27 November 2013 (dry season) onboard R/V "Tianlong". Sampling stations are indicated in Fig. 1. Detailed information about the sampling stations is provided in Appendix T1. A total of 6 stations were occupied along the salinity gradient in the PRE. Sediment cores were taken from a standard box corer ($20 \times 20 \times 60$ cm) and were checked visually to ensure that the interface was undisturbed. Overlying seawater samples (4 l) were collected from the box corer and were filtered

using a 142-mm 0.7 μm (nominal pore size) GFF filter. The filtrate and the particulate samples were obtained to determine seawater ^{224}Ra activity and to characterize the disequilibrium between ^{224}Ra and ^{228}Th in suspended particles. Sediment sub-samples were collected by inserting PVC tubes with a diameter of 47 mm into the bulk sediment core, and were subsequently analyzed for porosity, grain size, ^{224}Ra, ^{228}Th, as well as ^{234}Th in bulk sediments. Pore water was extracted from independent sediment sub-cores with a diameter of 65 mm using a Rhizon sampling device (Seeberg-Elverfeldt et al., 2005). Aliquots of ~15–20, ~5–10, and ~10 ml were extracted separately for the analyses of ^{224}Ra, DIC, and nutrients. In addition to sediment samples, surface seawater samples for the analyses of DIC and nutrients were collected with a higher spatial resolution using Niskin bottles attached on a CTD rosette sampler.

2.3. ^{224}Ra, ^{228}Th, and ^{234}Th analyses

^{224}Ra and ^{228}Th in bulk sediment/suspended particles were determined following the method described in Cai et al. (2012). In brief, the sediment sub-cores were sliced into 1-cm thick slabs immediately after sample collection. Milli-Q water was added to sediment slabs to form a slurry. Subsequently, $KMnO_4$ and $MnCl_2$ solutions were added to form a suspension of MnO_2, which serves to absorb dissolved ^{224}Ra in interstitial water. The MnO_2 suspension and the sediment with absorbed ^{224}Ra and ^{228}Th were filtered onto a 142-mm 0.7 μm (nominal pore size) GFF filter. The filter was placed onto a sample holder specified for sediment samples and counted for 4–6 h in a delayed coincidence counting system (the RaDeCC system). About 8–10 d later, the sample was re-counted using a same RaDeCC system. In order to verify the performance of the system, a third measurement was conducted ~25 d after sample collection. ^{224}Ra and ^{228}Th activities can be calculated either from the first and second measurements or from the first and third measurements. The RaDeCC system is calibrated with a ^{232}U–^{228}Th standard using the method of standard addition. It must be stressed that ^{224}Ra and ^{228}Th measurements based on this method represent the exchangeable ^{224}Ra fraction and the production rate of exchangeable ^{224}Ra in bulk sediment. For convenience, we will refer to these measurements as total ^{224}Ra and ^{228}Th activities as opposed to pore water ^{224}Ra measurements described below.

Pore water was extracted from two parallel sediment sub-cores (area = 33.2 cm^2) by inserting an array of Rhizon samplers directly into the sediment. Approximately 15–20 ml of pore water was retrieved at discrete depths in the sediment. The pore water sample was transferred into a 250 ml Teflon beaker and 150 ml of Milli-Q water was added. With addition of concentrated $NH_3{\cdot}H_2O$, the pH was adjusted to 8.0–9.0. Subsequently, 5.0 ml of $KMnO_4$ solution (3.0 g l^{-1}) and 5.0 ml of $MnCl_2$ solution (8.0 g $MnCl_2{\cdot}4H_2O$ l^{-1}) were added to form a suspension of MnO_2. The MnO_2 suspension was then filtered onto a 142-mm 0.7 μm GFF filter and counted in the RaDeCC system for ~10 h, which would generally result in a minimum of 100 counts in the channel 220. About 25 d later, a second measurement was performed to determine the background count rate of the sample due to ^{228}Th. Overlying seawater ^{224}Ra activity was determined in a manner similar to the measurement of pore water ^{224}Ra. The counting efficiency of ^{224}Ra is calibrated with a ^{232}U–^{228}Th standard that was prepared in the same manner as the sample.

Excess ^{234}Th (^{234}Th$_{ex}$) in the sediment was acquired from two parallel measurements. We have described our protocol most recently in Cai et al. (2014). It involves leaching of ^{234}Th from an initial sediment sample with a hot solution of 6 N HCl + H_2O_2, and purification of ^{234}Th based on the classical ion-exchange chemistry. ^{234}Th was co-precipitated with MnO_2 and determined by counting its daughter ^{234m}Pa on a gas-flow proportional low-level beta counter (GM-25-5, RISØ National Laboratory, Denmark). About 5–6 months after sample collection, a parallel sediment sample was processed and counted in the same manner as the initial sample. The overall yields of the procedure were determined using the method of standard addition.

2.4. DIC, nutrients, and TSM analyses

DIC samples were preserved with saturated $HgCl_2$. Within 2 weeks after sample collection, DIC was determined by Apollo Dissolved Inorganic Carbon Analyzer. This method has a precision of 0.1–0.2% (Cai et al., 2004; Guo et al., 2008). Certified reference materials from A. G. Dickson of Scripps Institution of Oceanography were used for DIC calibration.

Nutrient samples were stored at −20 °C until analysis except for NH_4^+, which was measured onboard with the indophenol blue spectrophotometric method (Dai et al., 2008). NO_3^- and NO_2^- measurements were based on the classical colorimetric methods and were conducted in our land-based laboratory at Xiamen University using a Four-channel Continuous Flow Technicon AA3 Auto-Analyzer (Bran-Lube GmbH). The detection limits for NO_3^-, NO_2^-, and NH_4^+ were 0.07, 0.02, and 0.16 μM, respectively.

For the determination of total suspended matter (TSM) concentrations, approximately 250–500 ml of seawater was filtered through a pre-weighed Nuclepore filter (0.45 μm). The filter was rinsed and dried at 60 °C until a constant weight was reached. The concentration of TSM was calculated from the weight difference between the sample and the filter.

3. RESULTS

Total and pore water ^{224}Ra, ^{228}Th, ^{234}Th$_{ex}$ activities as well as pore water DIC and nutrient concentrations in the near-surface sediments of the PRE are listed in Appendix T1. Sediment porosity, bottom water temperature and salinity as well as TSM at each station are also presented. Sediment ^{234}Th$_{ex}$ activity was calculated from the two parallel measurements and reported with a propagated uncertainty that includes the two parallel countings of

^{234}Th, the error of detector calibration, and the standard error of the overall yields. ^{224}Ra and ^{228}Th activities are reported with an error that was propagated from counting statistics, counter calibration, chance coincidence correction and in-growth/decay correction. We have compared the first and second measurements ($^{228}Th_{1,2}$) and the first and third measurements ($^{228}Th_{1,3}$) (Fig. 2). The results show that the mean ratio of $^{228}Th_{1,3}/^{228}Th_{1,2}$ is 1.01 ± 0.02 (1SD, $n = 66$), not significantly different from unity. In addition, the standard deviation is consistent with the counting statistics of an individual measurement of ^{228}Th (±2–3%). This suggests that counting statistics is the predominant source of error for the ^{224}Ra and ^{228}Th measurements. It must be noted that the final ^{228}Th activities are averages of $^{228}Th_{1,2}$ and $^{228}Th_{1,3}$. As such, we are confident that our method is very good and the difference between ^{224}Ra and ^{228}Th activities as shown in Fig. 3 is a real reflection of the deviation of ^{224}Ra relative to ^{228}Th in estuarine sediments.

3.1. Distributions of ^{224}Ra and ^{228}Th

Depth profiles of pore water ^{224}Ra, total ^{224}Ra, and ^{228}Th in the upper 0–15 cm sediment within the PRE are presented in Fig. 3. Pore water ^{224}Ra activity varied between 0.0011 ± 0.0014 and 0.056 ± 0.005 dpm ml^{-1}, which is ~1–2 orders of magnitude higher than ^{224}Ra activity in the overlying seawater. On average, however, it accounted for only 1.1% of the total desorbable ^{224}Ra activity in bulk sediment. In particular, pore water ^{224}Ra activity was low at the river mouth, where it constituted only ~0.2% of the total ^{224}Ra activity. This manifests the dramatically different geochemical characteristics of ^{224}Ra in freshwater vs. seawater. In freshwater, ^{224}Ra is bound strongly onto particle surfaces; however, as the ionic strength increases during mixing into seawater, desorption occurs and some ^{224}Ra is released (Swarzenski et al., 2003). Away from the river mouth, vertical profiles of pore water ^{224}Ra generally exhibited a maximum at the depth of 6–8 cm. Total ^{224}Ra activity in sediments ranged from 0.75 ± 0.03 to 3.20 ± 0.11 dpm g^{-1}. As ^{224}Ra is produced by ^{228}Th in sediments, vertical profiles of total ^{224}Ra generally showed a depth pattern similar to ^{228}Th. Sediment ^{228}Th activity fell in the range of 0.97 ± 0.03–3.34 ± 0.08 dpm g^{-1}, much higher than those observed in the Yangtze River Estuary (Cai et al., 2014). This could reflect the difference in sediment mineralogy and particle size between the two major estuaries in China. There was a general trend of decreasing ^{228}Th activity in the surface sediment from the inner to the outer estuary. Depth profiles of ^{228}Th collected from St. P03, A01, A04, and possible A09 showed a minimum at a certain depth (Fig. 3). Below this depth layer, ^{228}Th activity was relatively constant with depth. This depth pattern could be a result of the combination of ^{228}Th supply from the overlying water column via sinking particles coupled with a loss of ^{228}Ra from the upper sediment column. Depth profiles of sediment ^{228}Th collected from A04 and A06 showed a minimum in the surface sediment. This feature has also been observed in the Yangtze River Estuary and was ascribed to lateral transport of bottom sediment across the estuary (Cai et al., 2014).

As shown in Fig. 3, total ^{224}Ra was generally in deficit with respect to ^{228}Th in the near-surface sediments. The most marked deficit of total ^{224}Ra occurred in the mid-salinity region, where total ^{224}Ra/^{228}Th activity ratios (ARs) can be as low as ~0.40. Away from the mid-estuary, the depletion of total ^{224}Ra was less prominent. At the river mouth, ^{224}Ra deficit was confined in the upper 0–4 cm sediment; below this layer total ^{224}Ra approached secular equilibrium with ^{228}Th. In the high-salinity region, the total ^{224}Ra/^{228}Th AR in the sediment was generally >0.90.

Total ^{224}Ra and ^{228}Th activities in suspended particles ranged from 0.42 ± 0.04 to 6.09 ± 0.23 dpm g^{-1}, and from 0.79 ± 0.04 to 5.54 ± 0.21 dpm g^{-1}, respectively. At the river mouth, ^{224}Ra was in slight excess relative to ^{228}Th (Fig. 4). In the mixing zone, however, the ^{224}Ra/^{228}Th AR in suspended particles was well below 1, reflecting a marked depletion of ^{224}Ra. It fell in the range of 0.37–0.74, with an average of 0.53. This reveals that about 47% of the exchangeable ^{224}Ra in suspended particles was released during mixing into seawater. Seawater ^{224}Ra activity ranged from 22.6 ± 1.6 to 98.9 ± 3.9 dpm 100 l^{-1}, and showed a maximum in the mid-salinity region (Fig. 4). This mode of seawater ^{224}Ra vs. salinity is a common feature in estuaries. Finally, it is important to note that high seawater ^{224}Ra activity in the mid-salinity region coincides with the large deficit of total ^{224}Ra observed in bottom sediments.

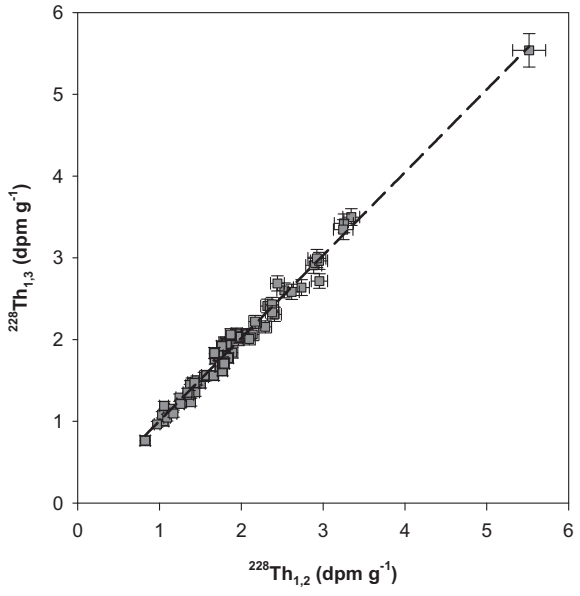

Fig. 2. Comparison of ^{228}Th activities based on the first and second measurements ($^{228}Th_{1,2}$), and on the first and third measurements ($^{228}Th_{1,3}$). The mean ratio of $^{228}Th_{1,3}/^{228}Th_{1,2}$ is 1.01 ± 0.02 (1SD, $n = 66$).

3.2. Excess ^{234}Th in the sediment

Excess ^{234}Th activity ($^{234}Th_{ex}$) was evident in the upper 0–3 cm sediment only at A01 and A09. $^{234}Th_{ex}$ activity in the surface 0–0.5 cm sediment ranged from 1.27 ± 0.12 to

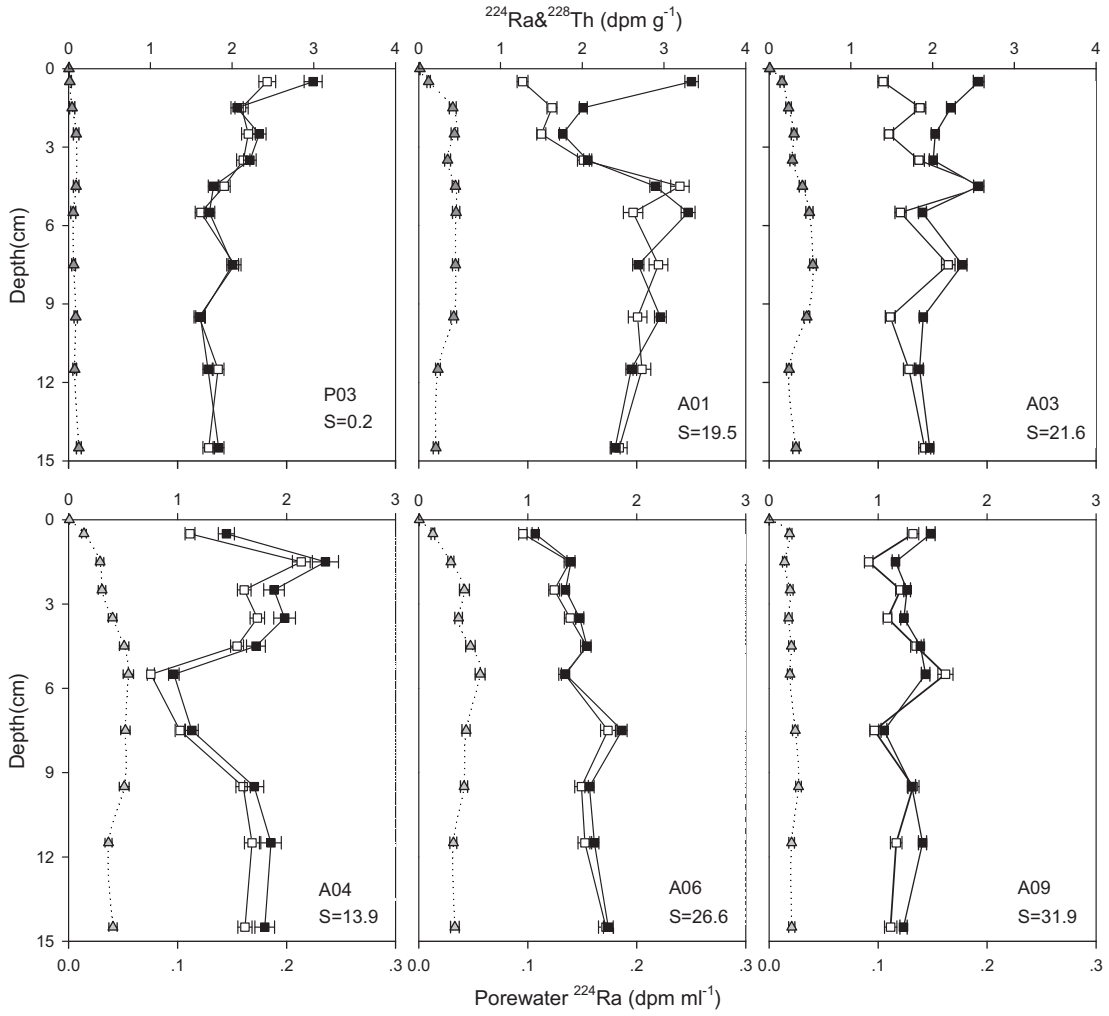

Fig. 3. Depth profiles of dissolved ^{224}Ra (filled triangle), total ^{224}Ra (open square), ^{228}Th (filled square) in the upper 0–15 cm sediment. Note that different coordinate scales are used in the upper panel and the lower panel to highlight the deficit of ^{224}Ra.

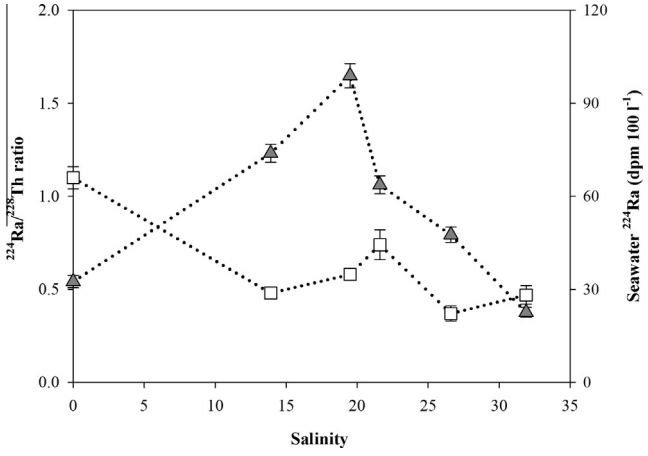

Fig. 4. Distributions of seawater ^{224}Ra activity (filled triangle) and ^{224}Ra/^{228}Th ratio on suspended particles (open square) along the salinity gradient in the Pearl River Estuary.

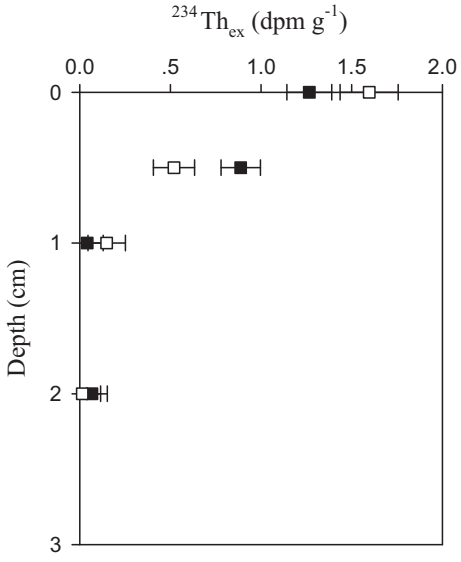

Fig. 5. Depth profiles of sediment $^{234}Th_{ex}$ collected at St. A01 (open square) and A09 (filled square).

1.60 ± 0.16 dpm g^{-1}. The $^{234}Th_{ex}$ profiles showed a decreasing excess with depth (Fig. 5). This must be ascribed to a balance of decay and penetration of $^{234}Th_{ex}$ into deeper sediment subsequent to its deposition over the seafloor. With a steady-state assumption, sediment mixing rates can be inferred from the depth profiles of $^{234}Th_{ex}$ (e.g., Aller and Cochran, 1976).

3.3. Distributions of DIC and nutrients

Depth profiles of pore water DIC, nitrate + nitrite (hereafter simply referred to as NO_3^-), and NH_4^+ in the upper 0–15 cm sediment are illustrated in Fig. 6. DIC and NH_4^+ contents varied from 1208 to 19,500 μM, and from 33 to 5410 μM, respectively. There was a general trend of decreasing DIC and NH_4^+ concentrations in pore water from the inner to the outer estuary. DIC and NH_4^+ normally increased with depth in the sediment. In contrast, NO_3^- was depleted within the upper ~3 cm sediment. In the inner estuary, depth profiles of pore water DIC and NH_4^+ were characterized by sharp concentration gradients. In comparison, the concentration gradients of pore water DIC and NH_4^+ were much less prominent in the mid- and outer estuary. Notably, the river core had an unusual low C:N ratio of ~3.2 in pore water below 1 cm sediment. This value is remarkably close to the C:N ratio of 3.3 that is characteristic of a process termed methanogenesis. Indeed, previous studies have shown that methane concentration in the surface water of the upper PRE can be as high as >2000 nM (e.g., Chen et al., 2008). This suggests that methane fermentation may dominate the organic break down in sediments at this site. From Fig. 6, one can also see DIC and NH_4^+ minima in pore water, which were probably a result of physical and/or bio-irrigation processes in the sediment.

NO_3^- and NH_4^+ concentrations in the surface waters varied from 6.9 to 258 μM, and from <0.25 to 414 μM, respectively. High NO_3^- and NH_4^+ contents were observed at the river mouth. Surface NO_3^- concentration decreased steadily during mixing into the open ocean, whereas NH_4^+ was efficiently removed close to the river mouth (Fig. 7).

4. DISCUSSION

4.1. Adsorption–desorption kinetics of ^{224}Ra

4.1.1. The diagenetic model for ^{224}Ra in sediments

In order to better utilize $^{224}Ra/^{228}Th$ disequilibrium as a proxy of solute transport processes across the sediment–water interface, it is essential to understand the reaction kinetics of ^{224}Ra in sediments. As we know, some ^{224}Ra produced by decay of ^{228}Th may enter the surrounding interstitial water. This soluble ^{224}Ra is then free to diffuse and, as a consequence, it migrates upward and outward resulting in a deficiency of total ^{224}Ra with respect to ^{228}Th in the upper portions of the sediments. A diagenetic model for the distributions of dissolved and adsorbed ^{224}Ra in sediments of the PRE can be constructed:

$$\frac{\partial(\phi Ra_d)}{\partial t} = \frac{\partial\left(\phi D_S \frac{\partial Ra_d}{\partial z}\right)}{\partial z} + \frac{\partial\left(D_B \frac{\partial(\phi Ra_d)}{\partial z}\right)}{\partial z} - I_{Ra} - \omega\frac{\partial(\phi Ra_d)}{\partial z} + (1-\phi)\rho_s S - \phi\lambda_{Ra} Ra_d \quad (1)$$

$$\frac{\partial[(1-\phi)\rho_s Ra_s]}{\partial t} = \frac{\partial\left(D_B \frac{\partial[(1-\phi)\rho_s Ra_s]}{\partial z}\right)}{\partial z} - \omega\frac{\partial[(1-\phi)\rho_s Ra_s]}{\partial z} - (1-\phi)\rho_s S + (1-\phi)\rho_s\lambda_{Ra}(Th - Ra_s) \quad (2)$$

where Ra and Th are ^{224}Ra and ^{228}Th activities in a unit of dpm g^{-1} dry mass, subscript d and s denote activities in pore water and on sediment particles; Note that Ra_d is defined as the concentration of Ra in dpm per volume of pore water; ϕ and ρ_s represent the sediment porosity and density; D_S is the diffusivity of ^{224}Ra in the sediment, D_B denotes the sediment mixing coefficient, ω is the sedimentation rate, and λ_{Ra} is the decay constant of ^{224}Ra; I_{Ra} represents the rate at which ^{224}Ra is transported out of the sediment by irrigation, and S is the net release rate of ^{224}Ra from sediment particles into the surrounding interstitial water. For the ^{224}Ra distribution in marine sediments, the advective burial of sediment is generally a negligible term (e.g., Hancock et al., 2000). With the assumption of constant ρ_s and D_B values with depth, the formulations for the steady-state distribution of ^{224}Ra in the sediment are written as:

$$\frac{\partial\left(\phi D_S \frac{\partial Ra_d}{\partial z}\right)}{\partial z} + \frac{\partial\left(D_B \frac{\partial(\phi Ra_d)}{\partial z}\right)}{\partial z} - I_{Ra} + (1-\phi)\rho_s S - \phi\lambda_{Ra} Ra_d = 0 \quad (3)$$

$$\frac{\partial\left(D_B \frac{\partial[(1-\phi)Ra_s]}{\partial z}\right)}{\partial z} - (1-\phi)S + (1-\phi)\lambda_{Ra}(Th - Ra_s) = 0 \quad (4)$$

In the above formulations, D_S is estimated from the molecular diffusion coefficient for radium in seawater (D) using the relation $D_S = D/\theta^2$, where θ denotes the sediment tortuosity and is derived from the porosity using the expression $\theta^2 = 1 - 2\ln(\phi)$ (Boudreau, 1997). D_B is inferred from

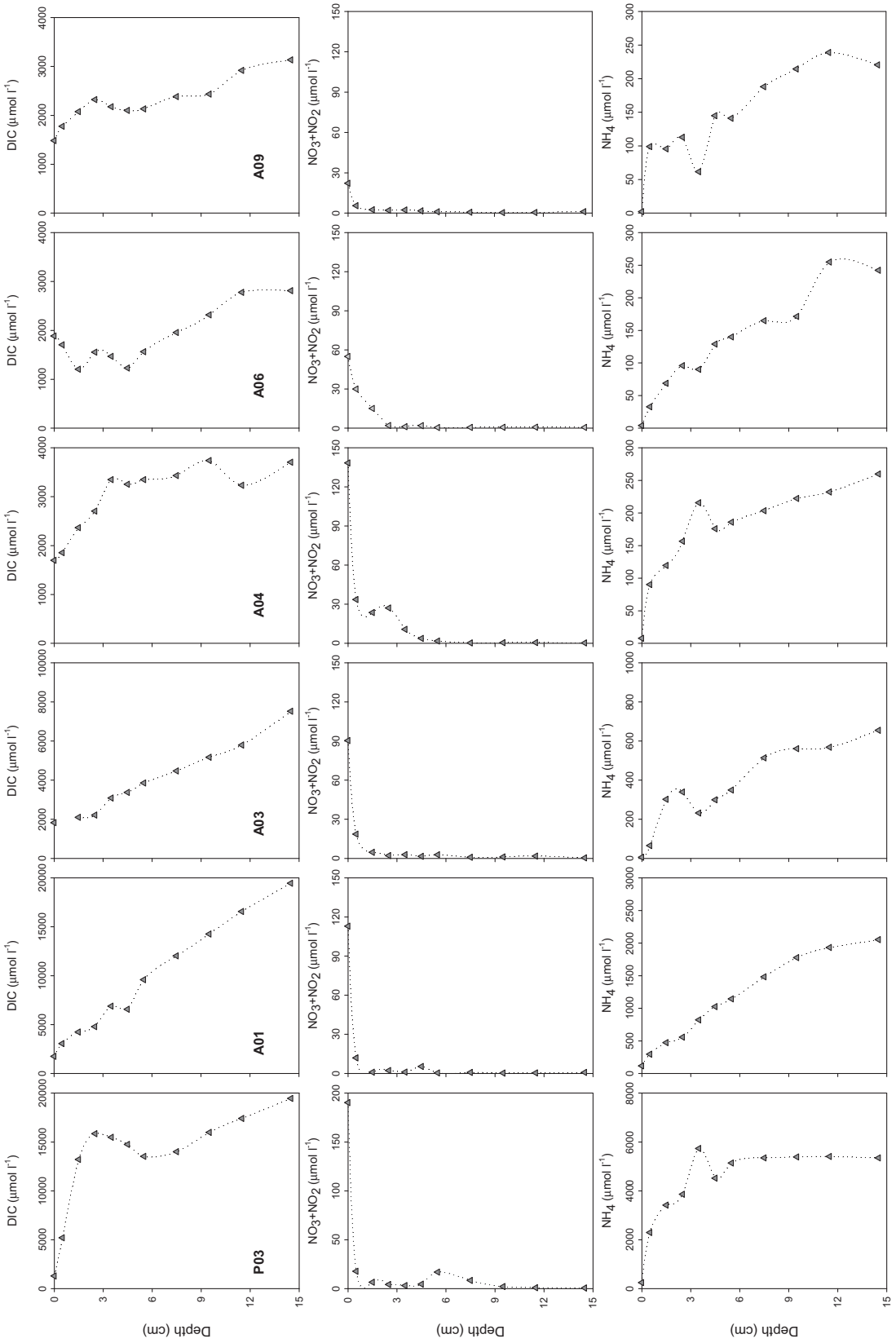

Fig. 6. Depth profiles of pore water DIC, $NO_2^- + NO_3^-$, and NH_4^+ in the upper 0–15 cm sediment. Note that different coordinate scales are used in each plot to highlight the gradient of concentration.

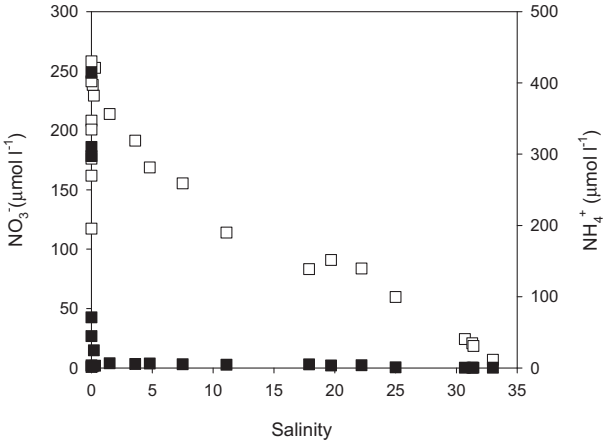

Fig. 7. Distributions of $NO_2^- + NO_3^-$ (open square) and NH_4^+ (filled square) in the surface water along the salinity gradient in the Pearl River Estuary.

the distributions of excess ^{234}Th in the upper sediment column. We derived a D_B value of 0.006 and 0.014 cm^2 d^{-1} for station A01 and A09, respectively. For the other stations where excess ^{234}Th was not detectable in the near-surface sediment, an average D_B value of 0.010 cm^2 d^{-1} was used to assess the role of sediment mixing in the mass balance of ^{224}Ra. The second derivatives $\frac{\partial\left(\phi D_S \frac{\partial Ra_d}{\partial z}\right)}{\partial z}$, $\frac{\partial\left(D_B \frac{\partial(\phi Ra_d)}{\partial z}\right)}{\partial z}$, and $\frac{\partial\left(D_B \frac{\partial[(1-\phi)Ra_S]}{\partial z}\right)}{\partial z}$ are computed from the depth distributions of dissolved and adsorbed ^{224}Ra in sediments using a numerical approach similar to that described in Ku et al. (1995). With this knowledge, the terms I_{Ra} and S can be calculated from Eqs. (3) and (4) for any specific depth in a sediment column.

4.1.2. Estimation of adsorption rate constants of ^{224}Ra

Recoil ejection accompanying its production by alpha decay in the solid particles has been recognized as a dominant source of short-lived uranium- and thorium-series radionuclides (such as ^{222}Rn and ^{224}Ra) in groundwater (e.g., Kigoshi, 1971; Krishnaswami et al., 1982). In addition to recoil ejection, adsorption and desorption of a radionuclide generally take place over a time scale of minutes and thus are important processes that affect the partition of ^{224}Ra between the aqueous phase and solid particles (e.g., Krishnaswami et al., 1982; Luo et al., 2000). If we assume that the kinetics of adsorption and desorption of ^{224}Ra are both a first-order process, then the term S in Eqs. (3) and (4) can be expressed as:

$$(1-\phi)\rho_s S = (1-\phi)\rho_s P + (1-\phi)\rho_s k_{-1} Ra_s - \phi k_1 Ra_d \quad (5)$$

where P denotes the ejection rate of ^{224}Ra to the aqueous phase by recoil; k_1 and k_{-1} represent the adsorption and desorption rate constant of ^{224}Ra. In order to determine k_1 and k_{-1} from Eq. (5), P and activities of two radium isotopes (e.g., ^{224}Ra–^{226}Ra or ^{224}Ra–^{228}Ra) must be known (Krishnaswami et al., 1982; Luo et al., 2000). Unfortunately, activities of a longer-lived radium isotope were not determined in this study. Nonetheless, we can use the measurements of ^{224}Ra and ^{228}Th on suspended particles to place a constraint on the supply terms of ^{224}Ra in sediment particles. As mentioned in Section 3.1, in the mixing zone of the PRE the total ^{224}Ra activities were considerably lower than the ^{228}Th activities on suspended particles. We may assume that the deficiency of ^{224}Ra on suspended particles was solely caused by the recoil ejection plus desorption of ^{224}Ra into seawater. Adsorption of dissolved ^{224}Ra onto suspended particles is supposed to be essentially zero, because of the low ^{224}Ra concentration and the high ionic strength in the water column. Consequently, the entire ^{224}Ra measurement on suspended particles represents the emanation rate (i.e., the ejection rate and the desorption rate). If we assume that the relative emanation rate of ^{224}Ra on sediment particles is similar to that on suspended particles in the overlying seawater, then Eq. (5) can be applied to sediment particles and takes the form:

$$(1-\phi)\rho_s S = (1-\phi)\rho_s \lambda_{Ra}(1-R_s)Th - \phi k_1 Ra_d \quad (6)$$

where R_s denotes the ^{224}Ra/^{228}Th AR for the sediment, as determined from suspended particles in the overlying seawater. With Eq. (6), knowledge of k_1 can be derived for any specific depth at a sediment column. For the station located at the river mouth (St. P03), the total ^{224}Ra activity was found to be in slight excess with respect to ^{228}Th on suspended particles (Fig. 4). This excess is considered to be a result of an increase in k_1 value in oxic freshwater. As such, we assume that the relative emanation rate of ^{224}Ra on suspended particles and sediment particles at this location is also similar to the rate on suspended particles in the mixing zone. An average R_s AR of 0.53 is thus assigned so as to estimate the adsorption rate constant of ^{224}Ra (k_1) at St. P03.

In the application of Eq. (6), however, it is important to note that suspended particles are probably finer-grained and the fraction of ^{224}Ra emanated may represent an upper limit of sediment particles. In such a case, k_1 would be overestimated. On the contrary, if R_s is smaller for sediment particles due to larger grain size, then k_1 would be underestimated. Despite of this limitation, the application of Eq. (6) would provide a first approximation of k_1 values of ^{224}Ra. The results show that for suspended particles in freshwater, k_1 is equal to 2000 ± 400 d^{-1}, or 1.4 ± 0.3 min^{-1}. This value is in agreement with previous results in oxic groundwater, which indicated that sorption of radium takes place on a time scale of minutes or less (e.g., Krishnaswami et al., 1982; Luo et al., 2000). For the sediment particles at the river mouth, k_1 varied between 25 ± 6 and 90 ± 70 d^{-1} (see Table 1), which is 1–2 orders of magnitude lower than the value derived for suspended particles in the overlying water. For the sediment samples collected in the mixing zone, k_1 was even lower, ranging from 0.1 ± 1.1 to 34 ± 4 d^{-1}. This reflects the decrease of the ^{224}Ra adsorption rate constant in high ionic strength seawater. We do not know what causes the difference in k_1 between the suspended particles and sediment particles at the river mouth. One plausible explanation may be related to the different redox conditions in the sediment column and in the overlying water. In comparison to the oxic

Table 1
Adsorption rate constant (k_1), retardation factor (R_f), observed flux of ^{224}Ra (F_{Ra}), theoretical flux of ^{224}Ra induced by molecular diffusion (F_M), by sediment mixing (F_B), and by irrigation (F_g) in the Pearl River Estuary.

Station	$^{*}k_1$ (d^{-1})	$^{*}R_f$	F_{Ra} (dpm cm^{-2} d^{-1})	F_M (dpm cm^{-2} d^{-1})	F_B (dpm cm^{-2} d^{-1})	F_g (dpm cm^{-2} d^{-1})
P03	25 ± 6–90 ± 70 (48 ± 22)	340 ± 90–2400 ± 600 (710 ± 660)	0.125 ± 0.070	0.0004 ± 0.0001	–	0.125 ± 0.070
A01	3.4 ± 0.9–34 ± 4 (12 ± 10)	58 ± 5–320 ± 30 (130 ± 80)	0.562 ± 0.081	0.0048 ± 0.0005	−0.0001 ± 0.0004	0.557 ± 0.081
A03	0.1 ± 1.1–7.4 ± 1.3 (4.0 ± 2.7)	35 ± 3–110 ± 10 (80 ± 26)	0.652 ± 0.046	0.0070 ± 0.0006	0.0006 ± 0.0007	0.644 ± 0.046
A04	0.9 ± 0.5–5.7 ± 2.0 (2.5 ± 1.4)	26 ± 2–190 ± 20 (99 ± 54)	0.656 ± 0.063	0.0040 ± 0.0004	0.0130 ± 0.0011	0.639 ± 0.063
A06	4.5 ± 0.6–9.8 ± 1.2 (7.4 ± 1.8)	40 ± 3–97 ± 12 (70 ± 17)	0.201 ± 0.054	0.0063 ± 0.0005	0.0077 ± 0.0006	0.187 ± 0.054
A09	5.2 ± 0.9–16.8 ± 2.0 (8.0 ± 3.5)	67 ± 7–140 ± 15 (97 ± 20)	0.260 ± 0.044	0.0093 ± 0.0006	0.0086 ± 0.0009	0.242 ± 0.044

* An average of all values at a station is presented in brackets. The error associated with the number represents a standard deviation of all the values.

overlying water, estuarine sediments are generally anoxic so that manganese oxides (MnO_2), a major carrier of ^{224}Ra, may be actively reduced to dissolved Mn^{2+}, thereby lowering the k_1 value of ^{224}Ra in sediments.

4.1.3. Calculation of partition coefficients and retardation factors of ^{224}Ra

Direct measurements of pore water ^{224}Ra and exchangeable ^{224}Ra on sediment particles also allow us to estimate the partition coefficient (K) and the retardation factor (R_f) for ^{224}Ra. These parameters are commonly expressed as:

$$K = \frac{\rho_s(1-\phi)\mathrm{Ra_s}}{\phi \mathrm{Ra_d}};\ \text{and}\ R_f = 1 + K \tag{7}$$

Results of the calculation show that values of R_f for sediments at the river mouth varied between 340 ± 90 and 2400 ± 630, with an average of 710 (see Table 1). In comparison, values of R_f for sediments in the mixing zone are much lower, ranging from 26 ± 2 to 320 ± 30. The average of all sediment samples collected in the mixing zone gives a R_f value of 96. The lower R_f values indicate that ^{224}Ra is more mobile in saline sediments than in fluvial sediments. Notably, the R_f values in this study are two orders of magnitude lower than previous results reported for oxic groundwaters (e.g., Krishnaswami et al., 1982; Luo et al., 2000). This may reflect the combined effect of redox conditions and the ionic strength on the mobility of ^{224}Ra in estuarine sediments. Nonetheless, our results are in good agreement with an R_f estimate of 112 that is inferred from a study of ^{222}Rn emanation rate (i.e., ^{226}Ra activity) in sandy sediments in Catalina Harbor, California (Colbert et al., 2008). Also, they are not inconsistent with laboratory determinations of K_d for Ra, which is defined as the ratio of Ra_s to Ra_d. Serene and Relyea (1982) reported that minimum values of K_d for Ra in granites, basalts, and tuffs are 50, 50, and 200 ml/g, respectively. If the porosity of sediment is 0.70, then the above K_d values give values of R_f in the range of 60 and 200, similar to the range of R_f determined using in situ ^{224}Ra measurements.

4.2. Benthic fluxes of ^{224}Ra

Outward fluxes of ^{224}Ra from bottom sediments in the PRE can be estimated using a one-dimensional (1D) mass balance exchange model (Cai et al., 2012). This model assumes that in-situ production via alpha decay of ^{228}Th is the sole source of ^{224}Ra in the sediment. At steady state, a mass balance consideration of ^{224}Ra in the sediment gives:

$$F_{Ra} = \int_0^{\infty} \lambda_{224}(A_{Th} - A_{Ra})dz \tag{8}$$

where F_{Ra} (dpm cm^{-2} d^{-1}) represents the flux of ^{224}Ra ("+" upward) across the sediment–water interface. A_{Th} and A_{Ra} are ^{228}Th and ^{224}Ra activities in bulk sediment (unit: dpm cm^{-3}). In practice, we assume that ^{224}Ra and ^{228}Th reach secular equilibrium below the sampling depth, i.e., 15 cm in this case. F_{Ra} was then calculated by trapezoidal integration of the ^{224}Ra deficit from 0 to 15 cm depth in the sediment. Results of the calculation show that outward fluxes of ^{224}Ra from bottom sediments

varied between 0.125 ± 0.070 and 0.656 ± 0.063 dpm cm^{-2} d^{-1} in our study region (Table 1). In addition, ^{224}Ra fluxes exhibited a plateau in the mid-salinity region. This pattern coincides with the mode of seawater ^{224}Ra vs. salinity in the water column, and suggests that pore water exchange could be a predominant source of the seawater ^{224}Ra in the PRE.

Like any dissolved species in sediment interstitial waters, outward fluxes of ^{224}Ra from bottom sediments are regulated by a variety of processes that operate at the sediment–water interface. Predominant processes include molecular diffusion, sediment mixing, and irrigation (e.g., Berner, 1980). The relative importance of these processes in regulating the ^{224}Ra flux has been evaluated by modeling the sediment ^{224}Ra profiles collected in the Yangtze River Estuary using the general diagenetic equation (Cai et al., 2014). A more direct approach, however, is to compare the theoretical fluxes induced by molecular diffusion and sediment mixing with the observed flux of ^{224}Ra. Given that the concentration gradient at the sediment–water interface can be computed from the depth profiles of pore water ^{224}Ra, we are thus able to calculate the fluxes of ^{224}Ra induced by molecular diffusion and sediment mixing using Fick's first law:

$$F_M = \phi D_S \left.\frac{\partial \mathrm{Ra_d}}{\partial z}\right|_{z=0}, \text{ and } F_B = D_B \left.\frac{\partial[\phi \mathrm{Ra_d} + \rho_s(1-\phi)\mathrm{Ra_s}]}{\partial z}\right|_{z=0} \quad (9)$$

where F_M and F_B denote the theoretical fluxes of ^{224}Ra induced by molecular diffusion and by sediment mixing, respectively. The concentration gradients $\frac{\partial \mathrm{Ra_d}}{\partial z}$ and $\frac{\partial[\phi \mathrm{Ra_d} + \rho_s(1-\phi)\mathrm{Ra_s}]}{\partial z}$ at the sediment–water interface, i.e., $z = 0$, are computed from the measurements in the overlying water and at the layer of 0–1 cm sediment. In regard to the ^{224}Ra flux induced by irrigation (F_g), we assume that it is equivalent to the difference between the observed flux derived from ^{224}Ra deficit and the theoretical fluxes caused by molecular diffusion plus sediment mixing. Results of the calculation show that values of F_M varied between 0.0004 ± 0.0001 and 0.0093 ± 0.0006 dpm cm^{-2} d^{-1} (Table 1), which on average accounted for only ~1.6% of the observed fluxes of ^{224}Ra. In comparison, values of F_B ranged from -0.0001 ± 0.0004 to 0.0130 ± 0.0011 dpm cm^{-2} d^{-1}, and were responsible for 0.0–3.8% of the measured fluxes of ^{224}Ra. Thus, molecular diffusion and sediment mixing can explain only <5% of the measured deficit of ^{224}Ra. This implies that the process of irrigation must be the dominant mechanism that controls outward fluxes of ^{224}Ra from bottom sediments in the PRE.

The importance of irrigation in regulating solute transfer across the sediment–water interface has been recognized in previous studies (e.g., Vanderborght et al., 1977; Aller, 1980; Huettel and Webster, 2001). In a recent study, we demonstrated that molecular diffusion was generally responsible for ~10% of the measured deficit of ^{224}Ra in the Yangtze River Estuary (Cai et al., 2014), which is an order of magnitude higher than the fraction identified in the present study. However, it must be noted that in the Yangtze River Estuary, only total ^{224}Ra activity in bulk sediment was determined. Under such a circumstance, we had to use a reference value of 11.7 for K_d so as to infer the concentration gradient of pore water ^{224}Ra at the sediment–water interface. Had the K_d value as measured in this study been used in the Yangtze River Estuary, the contribution of molecular diffusion to the total deficit of ^{224}Ra would have decreased from ~10% to ~2%. This value is remarkably close to the fraction determined in the PRE.

4.3. Transfer of DIC and nutrients across the sediment–water interface

In a most recent study, the ^{224}Ra/^{228}Th disequilibrium has been proposed as a new approach to determine the transfer rate of a dissolved species across the sediment–water interface (Cai et al., 2014). This approach, which we termed the ^{224}Ra/^{228}Th disequilibrium approach, is built upon the observed deficit of ^{224}Ra in the sediment and a concept of increased surface area for exchange by irrigation. The concept was proposed by early investigators and is now increasingly accepted in the field. In this concept, exchange of a dissolved species between the sediment and the overlying water is deemed to take place at a highly invaginated interface due to irrigation. In addition, molecular diffusion is assumed to be the predominant mechanism of transport at the interface. Consequently, the benthic flux of a dissolved species i (F_i) is expressed as (Cai et al., 2014):

$$F_i = F_{\mathrm{Ra}} \left(\frac{D_S^i}{D_S^{\mathrm{Ra}}}\right) \left(\frac{\frac{\partial c^i}{\partial z}}{\frac{\partial c^{\mathrm{Ra}}}{\partial z}}\right) \quad (10)$$

where superscript Ra and i denote ^{224}Ra and the dissolved species i, respectively; $\frac{\partial c}{\partial z}$ is the concentration gradient of the species of interest at the interface. Note that the ratio of molecular diffusion coefficient D_S^i/D_S^{Ra} in sediments is identical to the ratio in seawater, and is constant over the temperature range 0–25 °C that is generally encountered in the sediment (Boudreau, 1997).

The performance of the ^{224}Ra/^{228}Th disequilibrium approach relies on our ability to estimate the flux of ^{224}Ra, and how accurately we can characterize the concentration gradients of dissolved ^{224}Ra and the species of interest at the sediment–water interface. An important assumption associated with this approach is that the concentration gradients across the burrow wall are identical to those across the surficial sediment–water interface (Cai et al., 2014). In this regard, it must be pointed out that pore water ^{224}Ra, DIC, NO_3^- and NH_4^+ have rather different scale lengths. A consideration of the general diagenetic equation (e.g., see Eq. (10) in Cai et al., 2014) shows that relative to DIC and NH_4^+, pore water ^{224}Ra has a considerably small scale length such that its largest concentration gradient takes place over a few mm across the sediment–water interface. This difference is mainly caused by the kinetic nature of ^{224}Ra which, as elucidated in Section 4.1., leads to rapid adsorption of ^{224}Ra onto sediment particles. As such, high-resolution profiles of pore water ^{224}Ra are critically important for the application of the ^{224}Ra/^{228}Th disequilibrium approach. In this study, pore water ^{224}Ra, DIC, NO_3^-, and NH_4^+ concentrations were determined at

a depth interval of 1 cm in the upper sediment column. We use the measurements in the overlying water and at the layer of 0–1 cm sediment to estimate the term $\frac{\partial c^i}{\partial z}$ and $\frac{\partial c^{Ra}}{\partial z}$. The derived concentration gradients across the sediment–water interface are listed in Table 2. In particular, we find a strong correlation of DIC vs. dissolved ^{224}Ra and of NH_4^+ vs. dissolved ^{224}Ra in the upper several centimeters of sediments at some stations (Fig. 8). This level of correlation tends to support our assumption that the concentration gradients across the burrow wall are identical to those across the surficial sediment–water interface. Under such a circumstance, the benthic fluxes are most reliably determined using the ^{224}Ra/^{228}Th disequilibrium approach.

The benthic fluxes of DIC and nutrients were highly variable in the PRE, and in general, they spanned over a range of two orders of magnitude (Table 2). The DIC fluxes varied between -38 ± 12 and $8500 \pm 16{,}000$ mmol m^{-2} d^{-1} ("+" upward). In comparison, the NO_3^- and NH_4^+ fluxes ranged from -5 ± 1 to -660 ± 1200 mmol m^{-2} d^{-1}, and from 10 ± 3 to $7500 \pm 14{,}000$ mmol m^{-2} d^{-1}, respectively. Notably, all the highest fluxes were observed in the upper estuary (St. P03). Unfortunately, these estimates are associated with a very large uncertainty, which is mainly caused by the error associated with the measurement of pore water ^{224}Ra activity at the 0–1 cm sediment (see Appendix T1). As such, our later discussion will not be focused on these estimates. Away from the upper estuary into the mid-estuary, the fluxes diminished dramatically. It should also be noted that a negative flux of DIC was observed at St. A06, indicating a net removal of DIC from the overlying water column into bottom sediments. We do not know what caused the DIC removal at this location. Nonetheless, we have observed a lot of shells in the upper sediment column at this site. In addition, previous studies also showed that the benthic fauna at this location is characterized by high biomass of a mollusca species, *Potamocorbula laevis* (e.g., Huang et al., 2002). As such, we speculate that the DIC removal at this location may be caused by the formation of calcium carbonate in the top several centimeters of sediments, which could lower the DIC concentration in pore water and hence result in a negative gradient of DIC concentration across the sediment–water interface as shown in Fig. 6.

The benthic fluxes of DIC and nutrients from bottom sediments are expected to have a large impact on the biogeochemistry of the overlying water column. For a well-mixed water column, the benthic fluxes would induce a change of -4.3 ± 1.3 to 61 ± 16 μmol l^{-1}d^{-1} for DIC, of -0.2 ± 0.0 to -14 ± 3 μmol l^{-1} d^{-1} for NO_3^-, and of 1.2 ± 0.2 to 14 ± 4 μmol l^{-1} d^{-1} for NH_4^+ (see Table 2; "+" values denote net addition and "−" values represent net removal from the overlying water column). In the overlying water column, sources of DIC also include aerobic respiration and denitrification. In an earlier study, Guo et al. (2008) suggested that in the PRE aerobic respiration and denitrification would add DIC to the water column at a rate of 14–18, and of ~4 μmol l^{-1} d^{-1}, respectively. In the meantime, CO_2 evasion would remove DIC at a rate of 12–36 μmol l^{-1} d^{-1}. In terms of NH_4^+, Dai et al. (2008) demonstrated that in winter, nitrification would remove NH_4^+ at a rate of 0–5.4 μmol l^{-1} d^{-1}. At any rate, our

Table 2
Concentration gradient of dissolved ^{224}Ra, DIC, NO_3^-, and NH_4^+ at the sediment–water interface, and benthic fluxes ("+" upward) of DIC, NO_3^- and NH_4^+ in the Pearl River Estuary. Change rate (δ) of water column DIC, NO_3^- and NH_4^+ due to pore water exchange are also presented. Estimates with uncertainty >100% are highlighted in italic.

Station	∂Ra/∂z (dpm cm^{-4})	∂DIC/∂z (μmol cm^{-4})	$\partial NO_3^-/\partial z$ (μmol cm^{-4})	$\partial NH_4^+/\partial z$ (μmol cm^{-4})	DIC flux (mmol m^{-2} d^{-1})	NO_3^- flux (mmol m^{-2} d^{-1})	NH_4^+ flux (mmol m^{-2} d^{-1})	δDIC (μmol l^{-1} d^{-1})	δNO_3^- (μmol l^{-1} d^{-1})	δNH_4^+ (μmol l^{-1} d^{-1})
P03	*0.0015 ± 0.0028*	7.8	−0.38	4.1	*8500 ± 16000*	*−660 ± 1200*	*7500 ± 14000*	*940 ± 1800*	*−73 ± 140*	*830 ± 1600*
A01	0.016 ± 0.003	2.6	−0.22	0.36	1200 ± 300	−166 ± 42	278 ± 71	61 ± 16	−8.3 ± 2.1	14 ± 4
A03	0.023 ± 0.004	0.18	−0.14	0.12	70 ± 13	−87 ± 17	77 ± 15	10 ± 2	−13 ± 2	11 ± 2
A04	0.027 ± 0.004	0.31	−0.21	0.16	103 ± 19	−111 ± 20	91 ± 16	13 ± 2	−14 ± 3	11 ± 2
A06	0.025 ± 0.004	−0.36	−0.044	0.058	−38 ± 12	−8 ± 2	10 ± 3	−4.3 ± 1.3	−0.8 ± 0.3	1.2 ± 0.4
A09	0.038 ± 0.004	0.58	−0.033	0.20	54 ± 11	−5 ± 1	31 ± 6	2.1 ± 0.4	−0.2 ± 0.0	1.2 ± 0.2

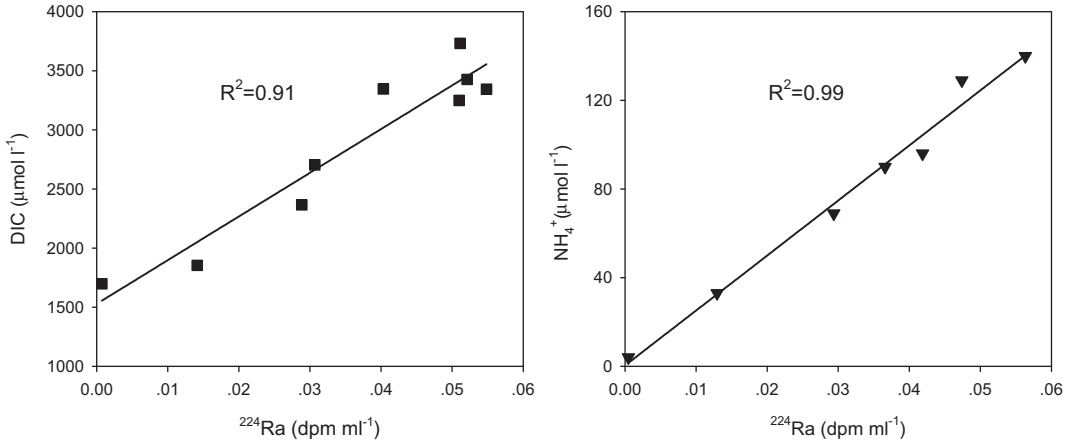

Fig. 8. Correlation of pore water DIC vs. dissolved ^{224}Ra in the upper 0–10 cm sediment interval at St.A04 (left panel), and of NH_4^+ vs. dissolved ^{224}Ra in the upper 0–6 cm sediment interval at St. A06 (right panel). Note that measurements in the overlying water are also included in the plots.

results suggest that pore water exchange is an important process and must be considered in the mass balance of DIC and nutrients in the Pearl River estuary.

Provided with a residence time of water mass, net addition or removal of water column DIC and nutrients due to pore water exchange can be assessed using the relation:

$$\Delta i = \frac{F_i \times \tau}{H} \tag{11}$$

where Δi refers to net addition or removal of a dissolved species from the overlying water column, τ is the water residence time in the estuary. Recently, Wang (2014) has utilized a tidal prism model (e.g., Sanford et al., 1992) to estimate water residence time in the PRE. This researcher derived a value of 2.2 ± 0.2 d in the wet season, and a value of 4.0 ± 1.4 d in the dry season. If we use an average of 3.0 d as the water residence time in November, a transition season in this region, then on average pore water exchange would lead to a change of 49 μmol l^{-1} for DIC, of -22 μmol l^{-1} for NO_3^-, and of 23 μmol l^{-1} for NH_4^+ in the water column of PRE. It is striking that bottom sediment removes water column NO_3^- at a rate remarkably close to the rate at which it adds NH_4^+ to the water column. If all the NH_4^+ added to the water column is nitrified, then the gain and loss of water column NO_3^- would be in balance. This may explain the quasi-conservative behavior of NO_3^- during estuarine mixing as shown in Fig. 7.

Total fluxes of DIC and nutrients due to pore water exchange can be estimated by integrating the site-specific fluxes over the whole PRE. Given the large uncertainty associated with the flux estimates at P03, we excluded this point and placed the other estimates onto a five-box grid with a total area of 1180 km^2, i.e., the area of the PRE. The choice of box dimensions was based on the estuary geometry. Box boundaries are shorelines, and demarcations that intersect the axis of the estuary. Box dimensions were determined from navigation charts. Consequently, the estuary is divided into five boxes with an area of 105, 179, 211, 383, and 302 km^2, respectively. The benthic fluxes as calculated from the ^{224}Ra/^{228}Th disequilibrium approach are multiplied by the sediment area to compute the flux from the sediments. Fluxes of DIC and nutrients at each box are added up. Assuming that our flux estimates are typical for the dry season (November−March), we would derive an annual flux of $42 \pm 6 \times 10^9$ mol yr^{-1} for DIC, of $-13 \pm 1 \times 10^9$ mol yr^{-1} for NO_3^-, and of $16 \pm 1 \times 10^9$ mol yr^{-1} for NH_4^+. The benthic flux of DIC is ~18% of the riverine input of DIC into the PRE, which was estimated to be $\sim 237 \times 10^9$ mol yr^{-1} in the dry season (Guo et al., 2008). During this cruise, NO_3^- and NH_4^+ concentrations at zero salinity spanned over a range of 104–319 and 1.3–414 μmol l^{-1}, respectively. Taking the medians as the end-member values and a discharge rate of 3600 m^3 s^{-1} (Cai et al., 2004), we would obtain a riverine flux of 9.1×10^9 mol yr^{-1} for NO_3^-, and of 3.1×10^9 mol yr^{-1} for NH_4^+ in the dry season. In this regard, our results indicate that bottom sediments are a major sink of water column NO_3^-, and are a predominant source of NH_4^+ in the PRE. It is interesting, however, to note that NO_3^- concentration in the surface water exhibited a quasi-conservative behavior, whereas NH_4^+ concentration in the surface water was almost depleted once it is away from the river mouth (Fig. 7). This pattern highlights the importance of water column processes, like nitrification and biological uptake, in regulating the concentration level of NO_3^- and NH_4^+ in the PRE (e.g., Dai et al., 2006,2008).

Total flux of DIC from bottom sediments into the PRE can also be deduced from a simple consideration of the mass balance of total organic carbon (TOC). As mentioned above, the PRE receives a delivery of $\sim 80 \times 10^6$ tons of sediments annually. Previous studies in the PRE suggest that TOC content in the surface sediments decreases from ~2.0–4.0% at the river mouth to ~1.0% in the lower estuary (e.g., Yang et al., 2011). On an annual basis, if we assume that 1.0–2.0% of TOC in the discharged sediments is combusted and converted to DIC, then we would derive a total flux of DIC:

$$F_{DIC} = 80 \times 10^{12} \text{ g yr}^{-1} \times (1.0\text{–}2.0\%)/12$$
$$= (67\text{–}134) \times 10^9 \text{ mmolC yr}^{-1}.$$

Appendix T1
Total and pore water ^{224}Ra (T. ^{224}Ra and P. ^{224}Ra), ^{228}Th, ^{234}Th$_{ex}$ activities as well as pore water DIC and nutrient concentrations in the near-surface sediments of the PRE.

Depth cm	Porosity	DIC (μmol l^{-1})	$NO_3^- + NO_2^-$ (μmol l^{-1})	NH_4^+ (μmol l^{-1})	P. ^{224}Ra (dpm ml^{-1})	T. ^{224}Ra (dpm g^{-1})	^{228}Th (dpm g^{-1})	^{224}Ra/^{228}Th A.R.	^{234}Th (dpm g^{-1})
**P03; 23° 04.452′N, 113° 28.218′E; 9.0 m; T = 20.9 °C, S = 0.2; TSM = 48.2 mg l^{-1}*									
Bottom water		1303	190.3	250	0.00033 ± 0.00002	6.09 ± 0.23	5.54 ± 0.21	1.10 ± 0.06	
0–1	0.705	5210	17.9	2300	0.0011 ± 0.0014	2.43 ± 0.10	2.99 ± 0.11	0.81 ± 0.05	ND
1–2	0.665	13,218	6.7	3419	0.0032 ± 0.0024	2.12 ± 0.08	2.06 ± 0.08	1.03 ± 0.05	ND
2–3	0.678	15,857	4.3	3861	0.0070 ± 0.0025	2.20 ± 0.08	2.33 ± 0.08	0.94 ± 0.05	ND
3–4	0.672	15,487	3.2	5739	ND	2.14 ± 0.08	2.22 ± 0.08	0.96 ± 0.05	ND
4–5	0.681	14,752	4.7	4523	0.0069 ± 0.0025	1.90 ± 0.07	1.77 ± 0.07	1.07 ± 0.06	ND
5–6	0.663	13,527	17.0	5145	0.0043 ± 0.0023	1.62 ± 0.07	1.72 ± 0.07	0.94 ± 0.05	ND
7–8	0.646	14,011	8.4	5352	0.0046 ± 0.0017	2.03 ± 0.08	2.03 ± 0.07	1.01 ± 0.05	ND
9–10	0.627	15,986	2.2	5394	0.0067 ± 0.0015	1.60 ± 0.06	1.61 ± 0.06	0.99 ± 0.05	ND
11–12	0.591	17,418	1.0	5407	0.0056 ± 0.0017	1.83 ± 0.07	1.71 ± 0.06	1.07 ± 0.06	ND
14–15	0.581	19,457	0.6	5352	0.0094 ± 0.0022	1.72 ± 0.07	1.84 ± 0.07	0.93 ± 0.05	ND
A01; 22° 44.222′N, 113° 39.257′E; 20.0 m; T = 21.5 °C, S = 19.5; TSM = 279 mg l^{-1}									
Bottom water		1755	113.0	117	0.00099 ± 0.00004	1.66 ± 0.07	3.42 ± 0.07	0.48 ± 0.02	
0–1	0.729	3070	12.0	296	0.0091 ± 0.0017	1.27 ± 0.07	3.34 ± 0.08	0.38 ± 0.02	1.60 ± 0.16
1–2	0.663	4253	1.0	474	0.031 ± 0.003	1.63 ± 0.06	2.01 ± 0.05	0.81 ± 0.04	0.52 ± 0.11
2–3	0.673	4795	2.3	557	0.033 ± 0.003	1.50 ± 0.06	1.76 ± 0.04	0.85 ± 0.04	0.15 ± 0.10
3–4	0.707	6886	1.1	825	0.027 ± 0.003	2.01 ± 0.07	2.07 ± 0.05	0.97 ± 0.04	0.01 ± 0.10
4–5	0.693	6573	5.4	1026	0.034 ± 0.003	3.20 ± 0.11	2.90 ± 0.07	1.10 ± 0.05	ND
5–6	0.689	9598	0.5	1145	0.034 ± 0.003	2.62 ± 0.12	3.30 ± 0.09	0.80 ± 0.04	ND
7–8	0.671	12,034	0.8	1482	0.034 ± 0.003	2.93 ± 0.12	2.69 ± 0.07	1.09 ± 0.05	ND
9–10	0.674	14,263	0.4	1778	0.032 ± 0.003	2.68 ± 0.11	2.96 ± 0.07	0.91 ± 0.04	ND
11–12	0.556	16,568	0.4	1932	0.018 ± 0.002	2.73 ± 0.11	2.60 ± 0.07	1.05 ± 0.05	ND
14–15	0.646	19,458	0.8	2054	0.016 ± 0.002	2.45 ± 0.10	2.40 ± 0.06	1.02 ± 0.05	ND
A03; 22° 36.411′N, 113° 42.581′E; 7.0 m; T = 21.2 °C, S = 21.6; TSM = 51.7 mg l^{-1}									
Bottom water		1828	90.4	5.9	0.00064 ± 0.00003	1.63 ± 0.07	2.84 ± 0.07	0.58 ± 0.03	
0–1	0.748	ND	18.6	66	0.012 ± 0.002	1.39 ± 0.06	2.56 ± 0.07	0.54 ± 0.03	ND
1–2	0.716	2103	4.7	302	0.018 ± 0.003	1.85 ± 0.07	2.22 ± 0.05	0.83 ± 0.04	ND
2–3	0.701	2216	2.2	340	0.023 ± 0.003	1.47 ± 0.06	2.03 ± 0.05	0.72 ± 0.03	ND
3–4	0.707	3087	2.9	232	0.021 ± 0.002	1.83 ± 0.07	2.01 ± 0.05	0.91 ± 0.04	ND
4–5	0.722	3372	1.7	300	0.030 ± 0.003	2.64 ± 0.09	2.56 ± 0.05	1.03 ± 0.04	ND
5–6	0.763	3849	2.8	350	0.037 ± 0.003	1.61 ± 0.07	1.88 ± 0.05	0.86 ± 0.04	ND
7–8	0.743	4469	0.9	514	0.040 ± 0.003	2.19 ± 0.08	2.36 ± 0.06	0.93 ± 0.04	ND
9–10	0.669	5167	1.2	562	0.035 ± 0.003	1.48 ± 0.06	1.88 ± 0.05	0.79 ± 0.04	ND
11–12	0.710	5787	1.9	569	0.018 ± 0.002	1.71 ± 0.07	1.84 ± 0.05	0.93 ± 0.04	ND
14–15	0.657	7511	0.5	656	0.025 ± 0.003	1.90 ± 0.07	1.97 ± 0.05	0.97 ± 0.04	ND
A04; 22° 31.195′N, 113° 44.481′E; 8.0 m; T = 22.3 °C, S = 13.9; TSM = 165 mg l^{-1}									
Bottom water		1698	138.5	7.9	0.00074 ± 0.00003	0.59 ± 0.06	0.79 ± 0.04	0.74 ± 0.08	
0–1	0.518	1854	33.7	90	0.014 ± 0.002	1.11 ± 0.05	1.45 ± 0.04	0.77 ± 0.04	ND
1–2	0.512	2366	23.7	120	0.029 ± 0.003	2.14 ± 0.08	2.36 ± 0.06	0.91 ± 0.04	ND
2–3	0.528	2704	27.1	157	0.031 ± 0.003	1.61 ± 0.06	1.89 ± 0.05	0.85 ± 0.04	ND

Appendix T1 (*continued*)

Depth cm	Porosity	DIC (μmol l^{-1})	$NO_3^- + NO_2^-$ (μmol l^{-1})	NH_4^+ (μmol l^{-1})	P. ^{224}Ra (dpm ml^{-1})	T. ^{224}Ra (dpm g^{-1})	^{228}Th (dpm g^{-1})	^{224}Ra/^{228}Th A.R.	^{234}Th (dpm g^{-1})
3–4	0.535	3347	10.8	216	0.040 ± 0.004	1.73 ± 0.07	1.98 ± 0.05	0.87 ± 0.04	ND
4–5	0.510	3249	3.8	176	0.051 ± 0.004	1.55 ± 0.06	1.72 ± 0.04	0.90 ± 0.04	ND
5–6	0.583	3344	1.8	186	0.055 ± 0.005	0.75 ± 0.03	0.97 ± 0.03	0.78 ± 0.04	ND
7–8	0.554	3427	0.3	204	0.052 ± 0.004	1.02 ± 0.04	1.13 ± 0.03	0.90 ± 0.05	ND
9–10	0.533	3732	0.5	222	0.051 ± 0.005	1.60 ± 0.07	1.70 ± 0.04	0.94 ± 0.05	ND
11–12	0.533	3226	0.7	232	0.037 ± 0.003	1.68 ± 0.07	1.86 ± 0.05	0.91 ± 0.04	ND
14–15	0.557	3698	0.3	260	0.041 ± 0.004	1.62 ± 0.07	1.80 ± 0.05	0.90 ± 0.04	ND
A06; 22° 23.486′N, 113° 46.497′E; 9.0 m; T = 23.1 °C, S = 26.6; TSM = 17.5 mg l^{-1}									
Bottom water		1886	55.0	4.0	0.00048 ± 0.00003	0.42 ± 0.004	1.12 ± 0.04	0.37 ± 0.04	
0–1	0.664	1707	33.0	33	0.013 ± 0.002	0.96 ± 0.04	1.07 ± 0.03	0.89 ± 0.04	ND
1–2	0.594	1208	15.2	69	0.029 ± 0.003	1.39 ± 0.05	1.40 ± 0.04	0.99 ± 0.05	ND
2–3	0.577	1554	2.1	96	0.042 ± 0.005	1.24 ± 0.05	1.36 ± 0.04	0.92 ± 0.04	ND
3–4	0.608	1468	1.2	90	0.037 ± 0.004	1.39 ± 0.05	1.48 ± 0.04	0.94 ± 0.04	ND
4–5	0.612	1231	2.0	129	0.047 ± 0.004	1.54 ± 0.06	1.54 ± 0.04	1.00 ± 0.04	ND
5–6	0.605	1567	0.5	140	0.056 ± 0.005	1.34 ± 0.06	1.35 ± 0.04	1.00 ± 0.05	ND
7–8	0.581	1956	0.6	165	0.043 ± 0.004	1.74 ± 0.07	1.87 ± 0.05	0.93 ± 0.04	ND
9–10	0.586	2318	0.7	172	0.042 ± 0.003	1.49 ± 0.06	1.57 ± 0.04	0.95 ± 0.05	ND
11–12	0.613	2780	0.8	255	0.032 ± 0.003	1.52 ± 0.06	1.61 ± 0.04	0.95 ± 0.05	ND
14–15	0.613	2814	0.6	242	0.033 ± 0.004	1.72 ± 0.07	1.74 ± 0.05	0.99 ± 0.05	ND
A09; 22° 12.046′N, 113° 48.795′E; 26.0 m; T = 22.7 °C, S = 31.9; TSM = 14.9 mg l^{-1}									
Bottom water		1484	22.2	2.4	0.00023 ± 0.00002	0.49 ± 0.05	1.02 ± 0.04	0.47 ± 0.05	
0–1	0.666	1774	5.6	99	0.019 ± 0.002	1.32 ± 0.05	1.48 ± 0.04	0.89 ± 0.04	1.27 ± 0.12
1–2	0.604	2075	2.5	96	0.014 ± 0.002	0.91 ± 0.04	1.16 ± 0.03	0.79 ± 0.04	0.89 ± 0.11
2–3	0.611	2319	2.1	113	0.019 ± 0.003	1.21 ± 0.04	1.27 ± 0.03	0.95 ± 0.04	0.04 ± 0.09
3–4	0.628	2174	2.4	62	0.018 ± 0.003	1.09 ± 0.04	1.24 ± 0.03	0.88 ± 0.04	0.07 ± 0.08
4–5	0.609	2097	1.7	145	0.021 ± 0.003	1.35 ± 0.05	1.39 ± 0.03	0.97 ± 0.04	ND
5–6	0.614	2127	1.1	141	0.019 ± 0.002	1.62 ± 0.07	1.44 ± 0.04	1.13 ± 0.06	ND
7–8	0.611	2376	0.7	188	0.024 ± 0.002	0.96 ± 0.04	1.05 ± 0.03	0.91 ± 0.05	ND
9–10	0.603	2428	0.4	215	0.027 ± 0.003	1.32 ± 0.05	1.31 ± 0.04	1.01 ± 0.05	ND
11–12	0.614	2910	0.5	239	0.021 ± 0.003	1.17 ± 0.05	1.41 ± 0.04	0.83 ± 0.04	ND
14–15	0.628	3125	1.2	221	0.021 ± 0.003	1.12 ± 0.06	1.23 ± 0.03	0.90 ± 0.05	ND

ND: Not detectable, i.e. when the second measurement of sediment ^{234}Th is larger or indistinguishable from the first measurement.

* T, S, and TSM represent temperature, salinity and total suspended matter concentration in the bottom water.

Guo et al. (2008) suggested that over an annual cycle (wet season + dry season), the Pearl River delivers $\sim 478 \times 10^9$ mmol yr^{-1} of DIC into the sea. In comparison, the flux of DIC from bottom sediments is ~14–28% of the riverine input of DIC. Our results based on the $^{224}Ra/^{228}Th$ disequilibrium approach in the dry season are in general agreement with the above estimate (18% vs. 14–28%).

5. CONCLUSIONS

The importance of pore water exchange in the overall budgets of water column DIC and nutrients in an estuary has long been recognized. Quantifying the benthic fluxes of these species, however, remains difficult due to limitations inherent in the traditional approaches, i.e., the benthic chamber method and the modeling approach. In this study, we have elaborated a newly developed approach – the $^{224}Ra/^{228}Th$ disequilibrium approach, to quantify the benthic fluxes of DIC and nutrients in a major estuary in China – the Pearl River Estuary (PRE). We demonstrate that irrigation was the predominant process that controls solute transfer across the sediment–water interface, whereas molecular diffusion and sediment mixing together accounted for <5% of the solute flux from bottom sediments. We show that sediment interstitial waters delivered approximately $42 \pm 6 \times 10^9$ mol of DIC and $\sim 16 \pm 1 \times 10^9$ mol of NH_4^+ into the PRE in the dry season. In contrast, it removed about $13 \pm 1 \times 10^9$ mol of NO_3^- from the overlying water column. Overall, our study highlights irrigation as an important process that controls the concentration levels of water column DIC and nutrients in estuaries.

We believe that the $^{224}Ra/^{228}Th$ disequilibrium approach is a very powerful tool for quantifying the rate of solute transfer across the sediment–water interface. In this study, we found that dissolved ^{224}Ra activities were generally well correlated with DIC and NH_4^+ concentrations in the upper several centimeters of sediments. Under such a circumstance, the $^{224}Ra/^{228}Th$ disequilibrium approach would provide very reliable flux estimates of DIC and NH_4^+. Future applications of the $^{224}Ra/^{228}Th$ disequilibrium approach may be extended to discern pore water exchange from submarine groundwater discharge (SGD) in estuarine and coastal environments. In terms of the methodology, inter-comparison between the $^{224}Ra/^{228}Th$ disequilibrium approach and the traditional approaches, such as a benthic chamber approach, should also be encouraged.

ACKNOWLEDGEMENTS

This work was supported by the Natural Science Foundation of China (NSFC) through grants 41276062 and 41576072, and by the National Major Scientific Research Project of China through Grant No. 2015CB954003. Support of this work also came from the National Basic Research Program ("973" program) of China (Grant No. 2014CB953702). We thank Dr. Yuwu Jiang for his help with calculating the area of the Pearl River Estuary. Nutrient samples in the surface water were analyzed by Lifang Wang. We thank W.S. Moore for helpful comments on an earlier version of this manuscript. Thanks are also due to M.M. Rutgers van der Loeff, W. Geibert, and an anonymous reviewer for their constructive comments. P.C. would like to dedicate this paper to BB for the inspiration of research.

APPENDIX

See Appendix T1.

REFERENCES

Aller R. C. (1980) Quantifying solute distributions in the bioturbated zone of marine sediments by defining an average microenvironment. *Geochim. Cosmochim. Acta* **44**, 1955–1965.

Aller R. C. and Cochran J. K. (1976) $^{234}Th/^{238}U$ disequilibrium in near-shore sediment: particle reworking and diagenetic time scales. *Earth Planet. Sci. Lett.* **29**, 37–50.

Berner R. A. (1980) *Early Diagenesis-A Theoretical Approach*. Princeton University Press, New Jersey.

Boudreau B. P. (1997) *Diagenetic models and their implementation: modelling transport and reactions in aquatic sediments*. Springer-Verlag, Berlin, Heidelberg, NY, pp. 414.

Cai W.-J., Dai M., Wang Y., Zhai W., Huang T., Chen S., Zhang F., Chen Z. and Wang Z. (2004) The biogeochemistry of inorganic carbon and nutrients in the Pearl River estuary and the adjacent Northern South China Sea. *Cont. Shelf Res.* **24**, 1301–1319.

Cai P., Shi X., Moore W. S. and Dai M. (2012) Measurement of $^{224}Ra:^{228}Th$ disequilibrium in coastal sediments using a delayed coincidence counter. *Mar. Chem.* **138**, 1–6.

Cai P., Shi X., Moore W. S., Peng S., Wang G. and Dai M. (2014) $^{224}Ra:^{228}Th$ disequilibrium in coastal sediments: implications for solute transfer across the sediment–water interface. *Geochim. Cosmochim. Acta* **125**, 68–84.

Chen C. T. A., Wang S. L., Lu X. X., Zhang S. R., Lui H. K., Tseng H. C., Wang B. J. and Huang H. I. (2008) Hydrogeochemistry and greenhouse gases of the Pearl River, its estuary and beyond. *Quatern. Int.* **186**, 79–90.

Colbert S. L., Berelson W. M. and Hammond D. E. (2008) Radon-222 budget in Catalina Harbor, California: 2. Flow dynamics and residence time in a tidal beach. *Limnol. Oceanogr.* **53**(2), 659–665.

Dai M., Guo X., Zhai W., Yuan L., Wang B., Wang L., Cai P., Tang T. and Cai W.-J. (2006) Oxygen depletion in the upper reach of the Pearl River estuary during a winter drought. *Mar. Chem.* **102**, 159–169.

Dai M., Wang L., Zhai W., Li Q., He B. and Kao S.-J. (2008) Nitrification and inorganic nitrogen distribution in a large perturbed river/estuarine system: the Pearl River Estuary, China. *Biogeosciences* **5**, 1227–1244.

Dai M., Gan J., Han A., Kung H. S. and Yin Z. Q. (2014) Physical dynamics and biogeochemistry of the Pearl River plume. In *Biogeochemical Dynamics at Major River-Coastal Interfaces: Linkages with Global Change* (eds. T. Bianchi, M. Allison and W.-J. Cai). Cambridge University Press, pp. 321–352.

Guo X., Cai W.-J., Zhai W., Dai M., Wang Y. and Chen B. (2008) Seasonal variations in the inorganic carbon system in the Pearl River (Zhujiang) estuary. *Cont. Shelf Res.* **28**, 1424–1434.

Hancock G. J., Webster I. T., Ford P. W. and Moore W. S. (2000) Using Ra isotopes to examine transport processes controlling benthic fluxes into a shallow estuarine lagoon. *Geochim. Cosmochim. Acta* **64**, 3685–3699.

He B., Dai M., Huang W., Liu Q., Chen H. and Xu L. (2010) Sources and accumulation of organic carbon in the Pearl River

Estuary surface sediment as indicated by elemental, stable carbon isotopic, and carbohydrate compositions. *Biogeosciences* **7**(10), 3343–3362.

Hensen C., Zabel M. and Schulz H. N. (2006) Benthic cycling of oxygen, nitrogen and phosphorus. In *Marine Geochemistry* (eds. H. D. Schulz and M. Zabel), second ed. Springer-Verlag, Berlin, Heidelberg, pp. 207–240.

Huang H., Lin Y., Li C., Lin Q., Cai W., Gao D. and Jia X. (2002) Ecology study on the benthic animals of the Pearl River estuary. *Acta Ecol. Sin.* **22**(2), 603–607 (In Chinese with English abstract).

Huettel M. and Webster I. T. (2001) Pore water flow in permeable sediments. In *The Benthic Boundary Layer – Transport Processes and Biogeochemistry* (eds. B. P. Boudreau and B. B. Jorgensen). Oxford University Press, Oxford, pp. 144–179.

Kigoshi K. (1971) Alpha-recoil Thorium-234: dissolution into water and the uranium-234/uranium-238 disequilibrium in nature. *Science* **173**, 47–48.

Knox S., Turner D., Dickson A., Liddicoat M., Whitfield M. and Butler E. (1981) Statistical analysis of estuarine profiles: application to manganese and ammonium in the Tamar Estuary. *Estuar. Coast. Shelf Sci.* **13**, 357–371.

Krishnaswami S., Graustein W. C., Turekian K. K. and Dowd J. F. (1982) Radium, thorium and radioactive lead isotopes in groundwaters: application to the in situ determination of adsorption–desorption rate constants and retardation factors. *Water Resour. Res.* **18**, 1663–1675.

Ku T. L., Luo S. D., Kusakabe M. and Bishop J. K. B. (1995) ^{228}Ra-derived nutrient budgets in the upper equatorial Pacific and the role of new silicate in limiting productivity. *Deep-Sea Res. Part II* **42**, 479–497.

Liu J. P., Xue Z., Ross K., Wang H. J., Yang Z. S., Li A. C. and Gao S. (2009) Fate of sediments delivered to the sea by Asian large rivers: long-distance transport and formation of remote alongshore clinothems. *Sed. Rec.* **7**(4), 4–9.

Lu Z. and Gan J. (2015) Controls of seasonal variability of phytoplankton blooms in the Pearl River Estuary. *Deep Sea Res. Part II* **117**, 86–96.

Luo S., Ku T.-L., Roback R., Murrell M. and McLing T. L. (2000) In-situ radionuclide transport and preferential groundwater flows at INEEL (Idaho): decay-series disequilibrium studies. *Geochim. Cosmochim. Acta* **64**, 867–881.

Mao Q., Shi P., Yin K., Gan J. and Qi Y. (2004) Tides and tidal currents in the Pearl River Estuary. *Cont. Shelf Res.* **24**, 1797–1808.

Sanford L. P., Boicourt W. C. and Rives S. R. (1992) Model for estimating tidal flushing of small embayments. *J. Waterw. Port Coast. Ocean Eng.* **118**, 635–654.

Seeberg-Elverfeldt J., Schluter M., Feseker T. and Kolling M. (2005) Rhizon sampling of porewaters near the sediment–water interface of aquatic systems. *Limnol. Oceanogr. Methods* **3**, 361–371.

Serene R. J. and Relyea J. F. (1982) The status of radionuclide sorption–desorption studies performed by the WRIT program. In *Rep. PNL-3977*. Pacific Northwest Laboratory, Richland, Wash., pp. 1–83.

Swarzenski P. W., Porcelli D., Andersson P. S. and Smoak J. M. (2003) The behavior of U- and Th-series nuclides in the estuarine environment. *Rev. Mineral. Geochem.* **52**, 577–606.

Vanderborght J. P., Wollast R. and Billen G. (1977) Kinetic models of diagenesis in disturbed sediments Part 1: mass transfer properties and silica diagenesis. *Limnol. Oceanogr.* **22**, 787–793.

Wang S. (2014) Submarine groundwater discharge and associated fluxes of nutrients and carbon into the Pearl River estuary. Master Thesis (in Chinese), Xiamen Univ., pp. 34–36.

Yang S., Tang M., Yim W. W.-S., Zong Y., Huang G., Switzer A. D. and Saito Y. (2011) Burial of organic carbon in Holocene sediments of the Zhujiang (Pearl River) and Changjiang (Yangtze River) estuaries. *Mar. Chem.* **123**, 1–10.

Zhang W., Zheng J., Ji X., Hoitink A. J. F., van der Vegt M. and Zhu Y. (2013) Surfical sediment distribution and the associated net sediment transport pattern in the Pearl River Estuary, South China. *Cont. Shelf Res.* **61–62**, 41–51.

Associate editor: Anthony Dosseto